

Temperature coefficients of phonon frequencies and thermal conductivity in thin black phosphorus layers

Liqin Su and Yong Zhang

Citation: [Applied Physics Letters](#) **107**, 071905 (2015); doi: 10.1063/1.4928931

View online: <http://dx.doi.org/10.1063/1.4928931>

View Table of Contents: <http://scitation.aip.org/content/aip/journal/apl/107/7?ver=pdfcov>

Published by the [AIP Publishing](#)

Articles you may be interested in

[Thermal diffusivity of electrical insulators at high temperatures: Evidence for diffusion of bulk phonon-polaritons at infrared frequencies augmenting phonon heat conduction](#)

J. Appl. Phys. **115**, 163517 (2014); 10.1063/1.4873295

[Phonon and thermal properties of exfoliated TaSe₂ thin films](#)

J. Appl. Phys. **114**, 204301 (2013); 10.1063/1.4833250

[Lower limit to phonon thermal conductivity of disordered, layered solids](#)

Appl. Phys. Lett. **94**, 181901 (2009); 10.1063/1.3127224

[Raman scattering on silicon nanowires: The thermal conductivity of the environment determines the optical phonon frequency](#)

Appl. Phys. Lett. **88**, 233114 (2006); 10.1063/1.2210292

[Photoluminescence and resonant Raman scattering in highly conductive ZnO layers](#)

Appl. Phys. Lett. **84**, 5168 (2004); 10.1063/1.1763980

An advertisement for the journal AIP APL Photonics. It features a cover image of the journal on the left, showing a blue and white abstract design. To the right of the cover is a yellow starburst graphic with the text 'OPEN ACCESS'. The main text reads 'Launching in 2016! The future of applied photonics research is here'. At the bottom right is the AIP APL Photonics logo. The background is a vibrant orange and red gradient with light flares.

Temperature coefficients of phonon frequencies and thermal conductivity in thin black phosphorus layers

Liqin Su and Yong Zhang^{a)}

Department of Electrical and Computer Engineering, University of North Carolina at Charlotte, Charlotte, North Carolina 28223, USA

(Received 13 May 2015; accepted 8 August 2015; published online 18 August 2015)

We investigate the temperature dependence of three major Raman modes of black phosphorus (BP) prepared by mechanical exfoliation from room temperature to 325 °C. With increasing temperature, all the Raman peaks show redshift in peak position and broadening in linewidth, but they depend on the film thickness. The first-order temperature coefficients of A_g^1 , B_{2g} , and A_g^2 are measured to be -0.0199 , -0.0304 , and -0.0321 cm^{-1}/K , respectively, in a ~ 20 -layer film. With decreasing thickness, the temperature coefficient decreases. The average thermal conductivity of a 70-nm thick BP film at room temperature is determined to be 15.8 W/mK when suspended, and 29.2 W/mK when supported on a SiO_2/Si substrate. Thermal decomposition temperature is found to be around 350 °C in N_2 environment. © 2015 AIP Publishing LLC.

[<http://dx.doi.org/10.1063/1.4928931>]

Two-dimensional (2D) layered materials, such as graphene and transition metal dichalcogenides (TMDs), have been intensively studied in the past decade with remarkable progress in the fields of electronic and optoelectronic applications.^{1–6} Although graphene reveals intriguing electronic, chemical, and mechanical properties, the lack of a band gap has made it difficult to be used in high-performance field effect transistors (FETs).⁷ Consequentially, seeking other 2D materials with a large band gap has attracted tremendous interest, including monolayer TMDs like MoS_2 , MoSe_2 , and WS_2 with bandgaps ranging from ~ 0.4 eV to ~ 2.3 eV,^{6,8–11} and black phosphorus (BP). In contrast to TMDs showing an abrupt change in bandgap with layer number,⁴ BP has a quasi-continuous layer-dependent bandgap varying from 0.3 eV for bulk to 1.5 eV for monolayer (i.e., phosphorene).^{12–16} Few-layer black phosphorus based FETs exhibit a hole mobility of ~ 1000 $\text{cm}^2 \text{V}^{-1} \text{s}^{-1}$ and on/off current ratio of 10^6 .¹⁶

As a promising material for applications in various electronic and optoelectronic devices, it is essential to understand the vibrational properties and electron-phonon interaction of black phosphorus. Raman spectroscopy has been used to investigate the vibrational and mechanical properties of layered materials.^{17,18} Furthermore, high temperature Raman study has been shown to be very effective for probing the 2D film/substrate interaction.^{18,19} In this work, we perform temperature dependent Raman studies on black phosphorus samples with different thicknesses in a temperature range from room temperature (RT) to 325 °C (close to the decomposition point). Additionally, by comparing the temperature dependence between suspended and supported BP, we are able to determine the substrate effect on the vibrational properties and thermal conductivity of BP.

Black phosphorus, the most stable form among phosphorus allotropes, is a layered material with weak interlayer bonding.^{20,21} BP or phosphorene has lower in-plane

symmetry compared to graphite and TMDs, resulting in its unique in-plane anisotropic nature.²¹ The space group of bulk BP is D_{2h} , and there are 12 lattice vibrational modes at Γ point, among which there six modes are Raman-active.²² However, only A_g^1 (out-of-plane mode), B_{2g} (in-plane mode along zigzag), and A_g^2 (in-plane mode along armchair) modes can be detected by Raman with back-scattering geometry according to symmetry selection rule.

High-quality BP crystals were purchased from Smart-Elements. BP flakes were obtained by mechanical exfoliation onto a silicon substrate coated with a 300 nm SiO_2 layer. Since BP is very sensitive to ambient environment, the sample was immediately (within 5 min) transferred into a heating chamber purging with nitrogen (N_2) gas for temperature dependent Raman measurements.²³ The flow rate of N_2 was low enough not to cause sample cooling. After Raman measurements were finished, tapping mode AFM was carried out to determine the thickness of exfoliated BP flakes. Micro-Raman measurements were performed with a Horiba LabRAM HR800 system using 532 nm excitation wavelength. A 1200 g/mm grating was used with a spectral resolution ~ 0.5 cm^{-1} . Laser power (density) was kept < 0.5 mW (measured at the exit of the microscope lens, $< 4 \times 10^4$ W/cm^2 with a $50 \times$ lens of $\text{NA} = 0.5$), without causing significant laser heating induced shift in Raman modes (e.g., 0.5 mW results in a ~ 0.5 cm^{-1} shift). Temperature dependent measurements were carried out in a 20 °C step using a heating system Linkam TS1500. At each temperature step, five minutes were allowed for thermal stabilization of the sample.

Figures 1(a)–1(c) show optical images of BP films with different thicknesses, which are labelled as samples S1–S4. Figure 1(d) shows the AFM image of samples S1 and S2 in Figure 1(a). The thickness of S1 is measured to be ~ 25 nm, while that of S2 is ~ 10 nm (~ 20 layers). The Raman spectra from all the four samples, measured with the same laser power at RT, are shown in Figure 1(e). Three typical Raman peaks corresponding to A_g^1 , B_{2g} , and A_g^2 are observed with their peak positions at ~ 362 , ~ 439 , and ~ 467 cm^{-1} ,

^{a)}yong.zhang@uncc.edu

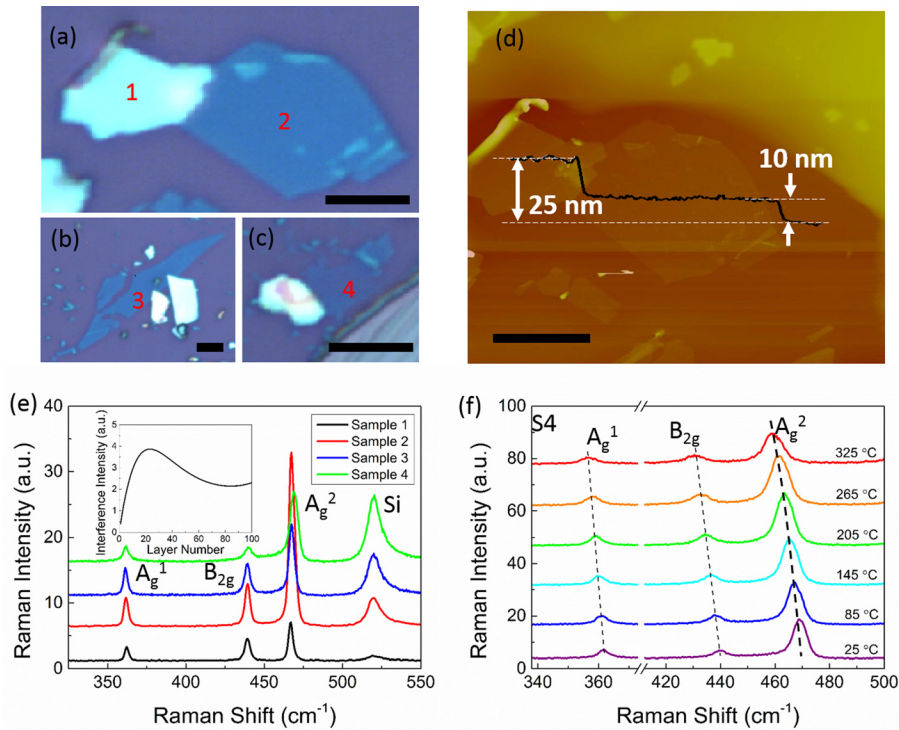


FIG. 1. (a)–(c) Optical images of BP flakes S1–S4. (d) AFM image of S1 and S2. (e) Raman spectra of sample S1–S4; inset: simulation of interference effect as a function of BP thickness. (f) Representative Raman spectra of S4 at different temperatures. All the scale bars are 5 μm .

respectively. These peaks were fitted with Lorentzian function. According to the intensity of silicon peak at 520 cm^{-1} , we can determine the thickness order of the four samples: $S1 > S2 > S3 > S4$ and estimate the thickness of S3 to be $\sim 6\text{ nm}$ and S4 $\sim 3\text{ nm}$. With decreasing thickness, A_g^2 shows a blueshift in frequency, A_g^1 mode a redshift, and B_{2g} mode almost no change. These thickness dependences are qualitatively similar to that of TMDs, where in-plane mode shows a blueshift and out-of-plane mode redshift, although for TMDs the shifts, due to interlayer interaction, occur when the films are only a few layers thick.^{24–26} Interestingly, the Raman intensities do not vary monotonically with thickness, with S2 being the strongest. This anomalous thickness dependence can be explained by optical interference with the model used in graphene and MoS_2 .^{27–29} The simulated results show that the film of ~ 20 layers exhibits the strongest intensity over a thickness range of 1–100 layers, which is in reasonably good agreement with experimental results (Figure 1(e)).

With increasing temperature, all Raman modes are expected to exhibit a redshift, as shown in Figure 1(f) by a few representative spectra of S4. The temperature shifts of Raman frequencies for the four samples are plotted in Figures 2(a)–2(c), respectively, for A_g^1 , B_{2g} , and A_g^2 , and fitted by a linear equation $\omega(T) = \omega_0 + \chi\Delta T$, where ω_0 is the Raman frequency at RT, χ is the first-order temperature coefficient, and ΔT is the temperature difference relative to RT. The change of Raman frequency with temperature can be caused by various anharmonic effects.¹⁷ The intrinsic linear dependence is usually valid for moderately high temperatures,³⁰ although for a 2D material the interaction with substrate may lead to significant distortion or nonlinearity.^{18,19} Therefore, high temperature data are more reliable for revealing the extrinsic effects due to, for instance, substrate. The obtained χ values for A_g^1 , B_{2g} and A_g^2 are listed in Table I. These values are substantially larger than those reported in the literature, presumably due to the differences

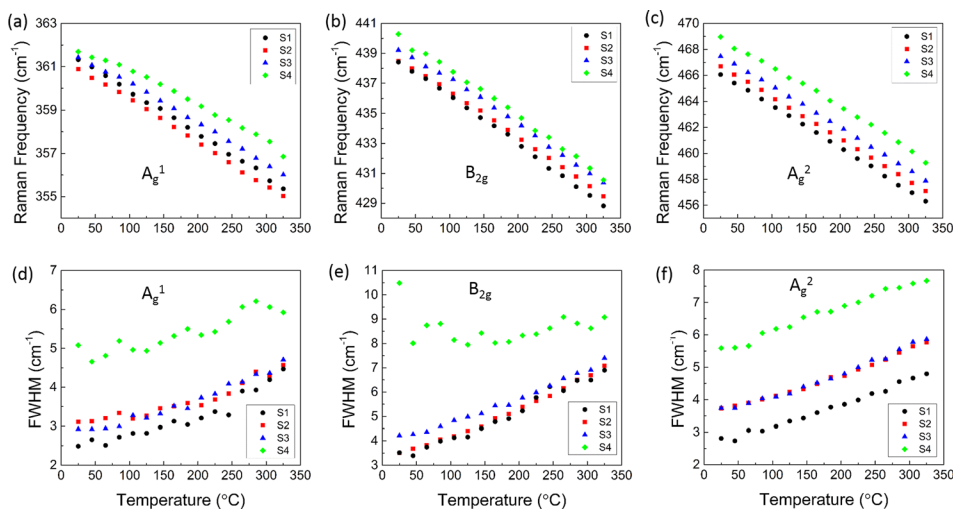


FIG. 2. (a)–(c) Temperature dependences of Raman frequencies of (a) A_g^1 , (b) B_{2g} , and (c) A_g^2 modes over a temperature range from RT to 325°C for sample S1–S4 on SiO_2 substrate. (d)–(f) Temperature dependences of FWHMs of (d) A_g^1 , (e) B_{2g} , and (f) A_g^2 modes in all the four samples.

TABLE I. Temperature coefficients (in cm^{-1}/K) of A_g^1 , B_{2g} , and A_g^2 modes of sample S1-S4, suspended and supported BP flakes.

	A_g^1	B_{2g}	A_g^2
Sample 1 (25 nm)	-0.0198	-0.0323	-0.0327
Sample 2 (10 nm)	-0.0198	-0.0304	-0.0324
Sample 3 (6 nm)	-0.0182	-0.0300	-0.0320
Sample 4 (3 nm)	-0.0158	-0.0315	-0.0312
Suspended (70 nm)	-0.0220	-0.0344	-0.0349
Supported (70 nm)	-0.0191	-0.0312	-0.0318

in measurement conditions, including laser power, temperature range, and environment.^{15,31}

Comparing the temperature coefficients of the four samples, we can see that the temperature coefficients of all the three modes in general decrease with decreasing thickness. As the thickness decreases, the BP film is more sensitive to its environment, such as substrate, which could lead to modifications of its intrinsic properties. All the four BP samples are held by SiO_2/Si substrate with relatively weak bonding, and the thermal expansion coefficient (TEC) of SiO_2 is much smaller than that of BP.³¹ With increasing temperature, the difference of TEC between the film and the substrate will introduce compressive strain to the film, which effectively reduce the intrinsic thermal expansion of lattice hence the redshift of Raman frequency. With increasing thickness, this effect tends to diminish. Thus, the thicker film like S1 is less susceptible to the substrate effect, leading to larger temperature coefficients than other thinner samples. Additionally, it is quite possible that ripples were introduced to BP films during the transfer process, showing a non-planar morphology especially when the film becomes thinner. The morphologic variation of the film, in particular, for very thin film, is the main origin of the strain. Based on our previous temperature-dependent Raman studies on TMDs, we have found that non-uniform morphology of the film can cause nonlinear temperature dependence for both in-plane and out-of-plane Raman modes.^{18,19} Among the four BP samples, all the three modes of the thinnest sample S4 clearly exhibit stronger nonlinear temperature dependence than the other three samples. As increasing temperature changes the strain in the film due to the TEC mismatch between the film and the substrate, the film will rearrange itself in morphology, which gives rise to nonlinear behavior of temperature dependence. For the thicker film, the morphology is expected to be more planar than other samples; thus, the temperature dependence is more linear.

The full width at half maximum (FWHM) of all the three modes increases with increasing temperature as shown in Figure 2(d)–2(f). At RT, the FWHM increases with decreasing thickness of BP film. For S4, the FWHM is almost double of other three samples. For instance, the FWHM values of S1 and S4 for A_g^1 mode are 2.5 ± 0.1 and $5.1 \pm 0.4 \text{ cm}^{-1}$, respectively, which are comparable to the literature values. This behavior can be explained by the effect related to variation in film morphology as discussed above. On increasing the thickness of the films, the effect of substrate is getting weaker and film morphology more uniform, hence smaller FWHM. For each individual sample,

with increasing temperature the FWHM increases. The broadening of Raman peaks typically involves the decay of an optical phonon into two acoustic phonons with the conservations of both momentum and energy.³⁰ However, the strain induced by the TEC mismatch coupled with the morphology inhomogeneity may also contribute to the broadening of Raman linewidth. The spectra of S1 and S2 before and after temperature-dependent Raman measurements are shown in Figure S1,³⁶ exhibiting no significant changes in its FWHM, which indicates that the strain effect is less important. It is worth noting that the decomposition of BP films is observed to occur at $\sim 350^\circ\text{C}$ in N_2 environment, manifested as a major reduction in Raman intensity and the sublimation of BP under visual observation. This is slightly lower than the reported thermal decomposition temperature of $\sim 400^\circ\text{C}$ under vacuum probed by other techniques.³¹

We further investigated the influence of substrate on temperature dependence by suspending the film. BP flakes were mechanically transferred onto a SiO_2/Si substrate (Figure 3(a)). A regular pattern of holes with a diameter of $10 \mu\text{m}$ was etched into the wafer. The thickness of the flake was determined to be $\sim 70 \text{ nm}$ by AFM. Figure 3(a) shows Raman spectra collected from the suspended (center of the hole) and supported regions at RT. Two noticeable differences are observed: (1) all the three modes in the suspended region are redshifted compared to supported region, due to heating as a result of lower thermal conductivity, and (2) the Raman intensity of suspended region is smaller than that of the supported region, due to an optical interference effect.²⁹ Temperature-dependent measurements were performed on both suspended and supported regions with the results for Raman frequencies shown in Figures 3(b)–3(d), and the temperature coefficients listed in Table I, indicating that the temperature coefficients of all the three modes in suspended region are greater in magnitude than those in supported region by $\sim 0.003 \text{ cm}^{-1}/\text{K}$ ($\sim 10\%$ – 15%). The difference cannot be explained by the residual laser heating effect, because the additional redshift induced by laser heating will not increase (but likely reduce) with increasing temperature. However, with increasing temperature, the supported BP film experiences compressive strain due to the TEC difference, leading to a blueshift which reduces the redshift caused by heating. For the suspended film, the potential strain caused by the larger thermal expansion of BP could be released through sagging of the film around the edge of the hole, resulting in a nearly strain-free state in the suspended region.

To investigate the laser heating effect more quantitatively, we carried out laser power dependent studies on both regions. The changes in the Raman spectra of suspended BP are shown in Figure 4(a). With increasing power, the peak positions of all the three modes redshift, indicating the local temperature rises. The frequency shifts are shown in Figures 4(b)–4(d), exhibiting that the slopes of the suspended region for all the three modes are larger than those of supported region by a factor of ~ 2.2 and the slope $\partial\omega/\partial P$ of A_g^1 mode is much smaller than those of the other two modes. The power used in the temperature-dependent Raman measurements was $\sim 0.5 \text{ mW}$, so we can calculate the temperature increase ΔT by the expression: $\Delta T = \Delta P \cdot (\partial\omega/\partial P) / (\partial\omega/\partial T)$, where ΔP is the highest laser power used and $\partial\omega/\partial T$ is the temperature

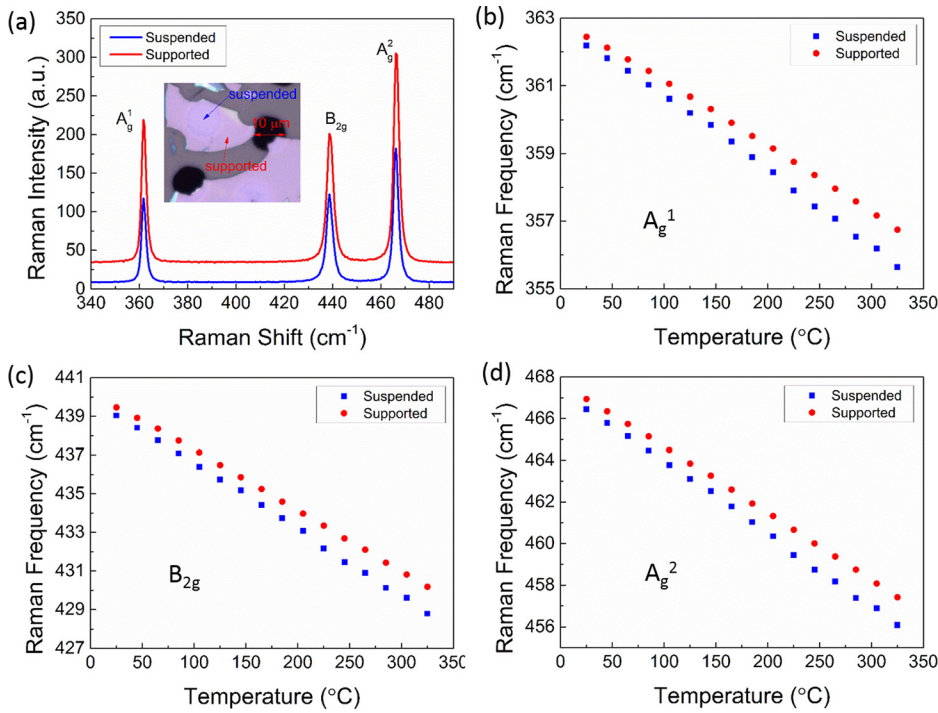


FIG. 3. (a) Raman spectra collected from suspended (blue) and supported (red) regions; inset: optical image of suspended BP flake. (b)–(d) Temperature dependences of Raman frequencies of (b) A_g¹, (c) B_{2g}, and (d) A_g² modes in suspended and supported regions.

coefficient. The temperature increases in suspended and supported regions are estimated to be ~ 22 and ~ 12 °C at $P = 0.5$ mW, respectively.

Finally, using the temperature and power dependent results obtained above, we can estimate the average thermal conductivity of BP. Because of the anisotropic nature of BP, the thermal conductivities are expected to be different between the zigzag armchair direction as k_{zig} and k_{arm} , and the average thermal conductivity can be viewed as $k = \sqrt{k_{zig}k_{arm}}$. Considering the thermal diffusion through an enclosed cylindrical surface in the suspended region, the average thermal conductivity can be evaluated using approximately using the formula below that has been developed for 2D materials^{32,33}

$$k = f\chi \frac{1}{2\pi h} \left(\frac{\partial \omega}{\partial P} \right)^{-1}, \quad (1)$$

where χ is the Raman temperature coefficient, h is the thickness of the film, and f is a reduction factor due to incomplete absorption of laser power. To the first order approximation, $f = g(1 - R)[1 - \exp(-\alpha h)]$, where g , R , and α are interference enhancement factor, reflectance of the BP top surface, and absorption coefficient of BP, respectively, which are all polarization dependent due to anisotropy. The crystalline orientation was determined by analyzing polarized Raman data,²¹ and the angle between the laser polarization and the zigzag direction was found to be $\sim 30^\circ$. (The angle-resolved

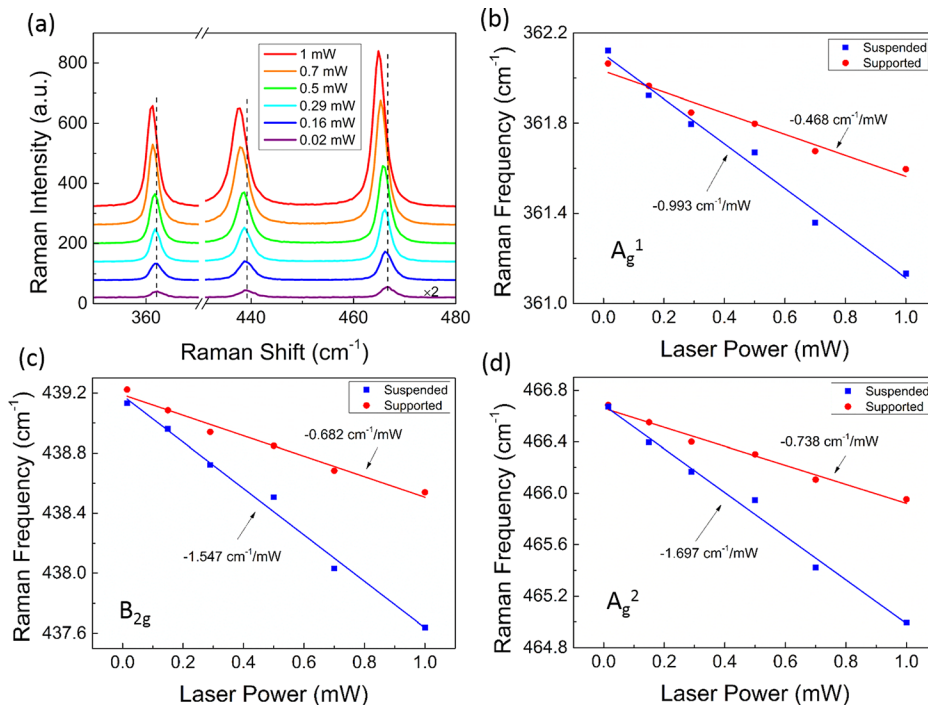


FIG. 4. (a) Raman spectra collected with different laser powers in suspended region. (b)–(d) Laser power dependences of Raman frequencies of (b) A_g¹, (c) B_{2g}, and (d) A_g² modes in suspended (blue) and supported (red) regions, including linear fits of experimental data.

Raman measurements are shown in Figure S2.)³⁶ The absorption coefficients and reflectance values were estimated for 532 nm with polarization in zigzag and armchair directions to be $\sim 5.5 \times 10^4 \text{ cm}^{-1}$ and $\sim 1.6 \times 10^5 \text{ cm}^{-1}$, $\sim 43.5\%$ and $\sim 44.4\%$, respectively.^{34,35} Thus, the f 's are estimated to be 0.23 and 0.21 for suspended and supported BP, respectively. Therefore, for the suspended region, the estimated average thermal conductivities are 16.1, 16.2, and 15.0 W/mK, using the parameters of A_g^1 , B_{2g} , and A_g^2 , respectively. These values, averaged to $k_{\text{susp}} = 15.8 \text{ W/mK}$, are in reasonable agreement with $k_{\text{arm}} \sim 20 \text{ W/mK}$, $k_{\text{zig}} \sim 40 \text{ W/mK}$ reported for BP thicker than 15 nm.³⁴ For the supported region, strictly speaking, Eq. (1) is not applicable. However, we may treat the substrate effect as a surface modification to the film and still use the equation to get an effective thermal conductivity. The results are 27.6 (A_g^1), 30.9 (B_{2g}), and 29.1 W/mK (A_g^2), respectively, and the average $k_{\text{supp}} = 29.2 \text{ W/mK}$. Although the thermal conductivity of SiO_2 , $\sim 1.4 \text{ W/mK}$, is much larger than $\text{N}_2 \sim 0.025 \text{ W/mK}$, it is still much smaller than that of BP. The significant enhancement in thermal conductivity seems to suggest that the supporting substrate plays a more subtle role than merely as a medium with a different thermal conductivity, for instance, the interface charges might significantly affect the thermal conductivity. This higher thermal conductivity at supported region can also explain the smaller temperature rise under high laser power in the supported region compared to suspended region. The obtained thermal conductivities for BP films are comparable to those for TMDs,^{33,35} but significantly smaller than graphene.³² The observed substrate effect is also applicable to other 2D materials.

In summary, temperature-dependent Raman scattering has been carried out to investigate the temperature effects in thin black phosphorus films with varying thicknesses prepared by mechanical exfoliation on SiO_2/Si substrate. We have found that the temperature dependence of the BP thin film is sensitive to the film thickness, showing a decreasing temperature coefficient with decreasing thickness. This behavior is attributed to the interaction of the film with substrate as well as the morphology distortion of the film. By studying a suspended film of 70 nm, we have obtained an average thermal conductivity of 15.8 W/mK for BP. Furthermore, we have shown that substrate can significantly affect the heat dissipation of the BP film, which yields a much larger effective thermal conductivity 29.2 W/mK. This work indicates that substrate can significantly impact the properties of the BP film, and the extent depends on the specific material property of interest for a given thickness.

We thank Professor L. Lew Yan Voon for assistance in acquiring the sample. Y.Z. acknowledges support of Bissell Distinguished Professorship.

¹K. S. Novoselov, A. K. Geim, S. V. Morozov, D. Jiang, Y. Zhang, S. V. Dubonos, I. V. Grigorieva, and A. A. Firsov, *Science* **306**(5696), 666 (2004).

²Y. Zhang, Y.-W. Tan, H. L. Stormer, and P. Kim, *Nature* **438**(7065), 201 (2005).

³A. K. Geim and K. S. Novoselov, *Nat. Mater.* **6**(3), 183 (2007).

⁴H. R. Gutiérrez, N. Perea-López, A. L. Elías, A. Berkdemir, B. Wang, R. Lv, F. López-Urías, V. H. Crespi, H. Terrones, and M. Terrones, *Nano Lett.* **13**(8), 3447 (2013).

⁵A. Splendiani, L. Sun, Y. Zhang, T. Li, J. Kim, C.-Y. Chim, G. Galli, and F. Wang, *Nano Lett.* **10**(4), 1271 (2010).

⁶B. Radisavljevic, A. Radenovic, J. Brivio, V. Giacometti, and A. Kis, *Nat Nanotechnol.* **6**(3), 147 (2011).

⁷I. Meric, M. Y. Han, A. F. Young, B. Ozyilmaz, P. Kim, and K. L. Shepard, *Nat Nanotechnol.* **3**(11), 654 (2008).

⁸S. Jo, N. Ubrig, H. Berger, A. B. Kuzmenko, and A. F. Morpurgo, *Nano Lett.* **14**(4), 2019 (2014).

⁹S. Das, H.-Y. Chen, A. V. Penumatcha, and J. Appenzeller, *Nano Lett.* **13**(1), 100 (2013).

¹⁰B. Chamlagain, Q. Li, N. J. Ghimire, H.-J. Chuang, M. M. Perera, H. Tu, Y. Xu, M. Pan, D. Xao, J. Yan, D. Mandrus, and Z. Zhou, *ACS Nano* **8**(5), 5079 (2014).

¹¹H.-J. Chuang, X. Tan, N. J. Ghimire, M. M. Perera, B. Chamlagain, M. M.-C. Cheng, J. Yan, D. Mandrus, D. Tománek, and Z. Zhou, *Nano Lett.* **14**(6), 3594 (2014).

¹²H. Liu, A. T. Neal, Z. Zhu, Z. Luo, X. Xu, D. Tománek, and P. D. Ye, *ACS Nano* **8**(4), 4033 (2014).

¹³M. Buscema, D. J. Groenendijk, S. I. Blanter, G. A. Steele, H. S. J. van der Zant, and A. Castellanos-Gomez, *Nano Lett.* **14**(6), 3347 (2014).

¹⁴T. Hong, B. Chamlagain, W. Lin, H.-J. Chuang, M. Pan, Z. Zhou, and Y.-Q. Xu, *Nanoscale* **6**(15), 8978 (2014).

¹⁵S. Zhang, J. Yang, R. Xu, F. Wang, W. Li, M. Ghufuran, Y.-W. Zhang, Z. Yu, G. Zhang, Q. Qin, and Y. Lu, *ACS Nano* **8**(9), 9590 (2014).

¹⁶L. Li, Y. Yu, G. J. Ye, Q. Ge, X. Ou, H. Wu, D. Feng, X. H. Chen, and Y. Zhang, *Nat Nano* **9**(5), 372 (2014).

¹⁷I. Calizo, A. A. Balandin, W. Bao, F. Miao, and C. N. Lau, *Nano Letters* **7**(9), 2645 (2007).

¹⁸L. Su, Y. Zhang, Y. Yu, and L. Cao, *Nanoscale* **6**(9), 4920 (2014).

¹⁹L. Su, Y. Yu, L. Cao, and Y. Zhang, "Effects of substrate type and material-substrate bonding on high-temperature behavior of monolayer WS_2 ," *Nano Res.* (to be published).

²⁰F. Bachhuber, J. von Appen, R. Dronskowski, P. Schmidt, T. Nilges, A. Pfitzner, and R. Wehrich, *Angew. Chem. Int. Ed.* **53**(43), 11629 (2014).

²¹J. Wu, N. Mao, L. Xie, H. Xu, and J. Zhang, *Angew. Chem. Int. Ed.* **54**(8), 2366 (2015).

²²S. Sugai, T. Ueda, and K. Murase, *J. Phys. Soc. Jpn.* **50**(10), 3356 (1981).

²³J. D. Wood, S. A. Wells, D. Jariwala, K.-S. Chen, E. Cho, V. K. Sangwan, X. Liu, L. J. Lauhon, T. J. Marks, and M. C. Hersam, *Nano Lett.* **14**(12), 6964 (2014).

²⁴A. G. Bagnall, W. Y. Liang, E. A. Marseglia, and B. Welber, *Physica B+C* **99**(1-4), 343 (1980).

²⁵H. Li, Q. Zhang, C. C. R. Yap, B. K. Tay, T. H. T. Edwin, A. Olivier, and D. Baillargeat, *Adv. Funct. Mater.* **22**(7), 1385 (2012).

²⁶C. Lee, H. Yan, L. E. Brus, T. F. Heinz, J. Hone, and S. Ryu, *ACS Nano* **4**(5), 2695 (2010).

²⁷C. Casiraghi, A. Hartschuh, E. Lidorikis, H. Qian, H. Harutyunyan, T. Gokus, K. S. Novoselov, and A. C. Ferrari, *Nano Lett.* **7**(9), 2711 (2007).

²⁸S.-L. Li, H. Miyazaki, H. Song, H. Kuramochi, S. Nakaharai, and K. Tsukagoshi, *ACS Nano* **6**(8), 7381 (2012).

²⁹M. Buscema, G. Steele, H. J. van der Zant, and A. Castellanos-Gomez, *Nano Res.* **7**(4), 561 (2014).

³⁰J. Menéndez and M. Cardona, *Phys. Rev. B* **29**(4), 2051 (1984).

³¹X. Liu, J. D. Wood, K.-S. Chen, E. Cho, and M. C. Hersam, *J. Phys. Chem. Lett.* **6**(5), 773 (2015).

³²A. A. Balandin, S. Ghosh, W. Bao, I. Calizo, D. Teweldebrhan, F. Miao, and C. N. Lau, *Nano Lett.* **8**(3), 902 (2008).

³³N. Peimyo, J. Shang, W. Yang, Y. Wang, C. Cong, and T. Yu, *Nano Res.* **8**(4), 1210 (2015).

³⁴Z. Luo, J. Maassen, Y. Deng, Y. Du, M. S. Lundstrom, P. D. Ye, and X. Xu, preprint [arXiv:1503.06167](https://arxiv.org/abs/1503.06167) [cond-mat] (2015).

³⁵S. Sahoo, A. P. S. Gaur, M. Ahmadi, M. J. F. Guinel, and R. S. Katiyar, *J. Phys. Chem. C* **117**(17), 9042 (2013).

³⁶See supplementary material at <http://dx.doi.org/10.1063/1.4928931> for more details: Raman spectra collected before and after the temperature-dependent Raman measurements, and angle-resolved Raman spectroscopy of the suspended BP film.